## REPORT

#### **QUANTUM GASES**

# Two- and three-body contacts in the unitary Bose gas

Richard J. Fletcher, \*\* Raphael Lopes, \*1 Jay Man, \*1 Nir Navon, \*1 Robert P. Smith, \*1 Martin W. Zwierlein, \*2 Zoran Hadzibabic\*\*

In many-body systems governed by pairwise contact interactions, a wide range of observables is linked by a single parameter, the two-body contact, which quantifies two-particle correlations. This profound insight has transformed our understanding of strongly interacting Fermi gases. Using Ramsey interferometry, we studied coherent evolution of the resonantly interacting Bose gas, and we show here that it cannot be explained by only pairwise correlations. Our experiments reveal the crucial role of three-body correlations arising from Efimov physics and provide a direct measurement of the associated three-body contact.

fundamental challenge in many-body quantum physics is to connect the macroscopic behavior of a system to the microscopic interactions between its constituents. In ultracold atomic gases, the strength of interactions is most commonly characterized by the s-wave scattering length a, which can be tuned by using Feshbach resonances (I). On resonance, a diverges and the unitary regime is reached, in which the interactions are as strong as allowed by quantum mechanics. This regime has been extensively studied in Fermi gases (2–4), whereas the unitary Bose gas represents a new experimental and theoretical frontier (5–II).

In gases interacting via pairwise contact interactions, universal properties of the short-range particle correlations imply universal thermodynamic relations between macroscopic observables such as the momentum distribution, energy, and spectroscopic response (12-20). In the case of (mass-balanced) two-component Fermi gases, at the heart of these relations is a single fundamental thermodynamic parameter, the two-body contact density  $C_2$ , which measures the strength of twoparticle correlations. However, the case of the Bose gas is more subtle because of the lack of the Pauli exclusion principle, which governs the behavior of identical fermions. In this system, Efimov physics gives rise to three-body bound states (21-27) and more generally introduces threeparticle correlations that cannot be deduced from the knowledge of pairwise ones (18-20, 28). The implication for many-body physics is that complete understanding of the macroscopic coherent phenomena requires knowledge of both  $C_2$  and its three-body analog  $C_3$  (18-20).

<sup>1</sup>Cavendish Laboratory, University of Cambridge, J. J. Thomson Avenue, Cambridge CB3 OHE, UK. <sup>2</sup>Department of Physics, MIT-Harvard Center for Ultracold Atoms, and Research Laboratory of Electronics, Massachusetts Institute of Technology, Cambridge, MA 02139, USA.

\*Corresponding author. Email: rfletch@mit.edu

The relative importance of three-particle correlations generally grows with the strength of interactions. At moderate interaction strengths,  $C_2$  has been measured spectroscopically, but  $C_3$  has not been observed (25). However, the momentum distribution of the unitary Bose gas (7) has suggested deviations from two-body physics (20, 29).

We interferometrically measured both  $C_2$  and  $C_3$  in a resonantly interacting thermal Bose gas. The idea of our experiment is illustrated in

Fig. 1. We performed radio-frequency (RF) Ramsey interferometry on a gas of atoms with two internal (spin) states, ↑ and ⊥, and used a magnetic Feshbach resonance to enhance ↑↑ interactions; both  $\uparrow\downarrow$  and  $\downarrow\downarrow$  interactions are negligible. For a measurement at a given magnetic field, we initially prepared a gas in the ↓ state and then used a RF pulse to put each atom into an equal superposition of  $\uparrow$  and  $\downarrow$ . This corresponded to an interaction quench that initiated many-body dynamics. During the subsequent evolution, the ↑ component of an atom's wave function accumulated a phase  $\phi$  because of interactions with the other ↑ components in the surrounding cloud. As we formally show (30), the rate at which  $\varphi$ accumulates reflects many-body correlations that would develop in a purely ↑ system with half the total density. Meanwhile, the ↓ component serves as a noninteracting phase reference, which allows us to read out  $\varphi$  interferometrically. This was accomplished by a second RF pulse, which mapped φ onto a spin-population imbalance that we measured directly. Recently, similar methods have been used to study impurities in a Fermi

In the bottom row of Fig. 1, the steps of our protocol are shown on the Bloch sphere, in terms of the collective spin  $\vec{S}$ . During the evolution of the equal-superposition state,  $\vec{S}$  precesses with time, t, in the equatorial plane at a rate  $\Omega = \partial \phi / \partial t$ . We derive the following relationship between  $\Omega$  and the two- and three-body contacts (30)

$$\Omega = \frac{\hbar}{4\pi m} \left( \frac{1}{na} C_2 + \frac{5.0 \,\pi^2}{n} C_3 \right) \tag{1}$$

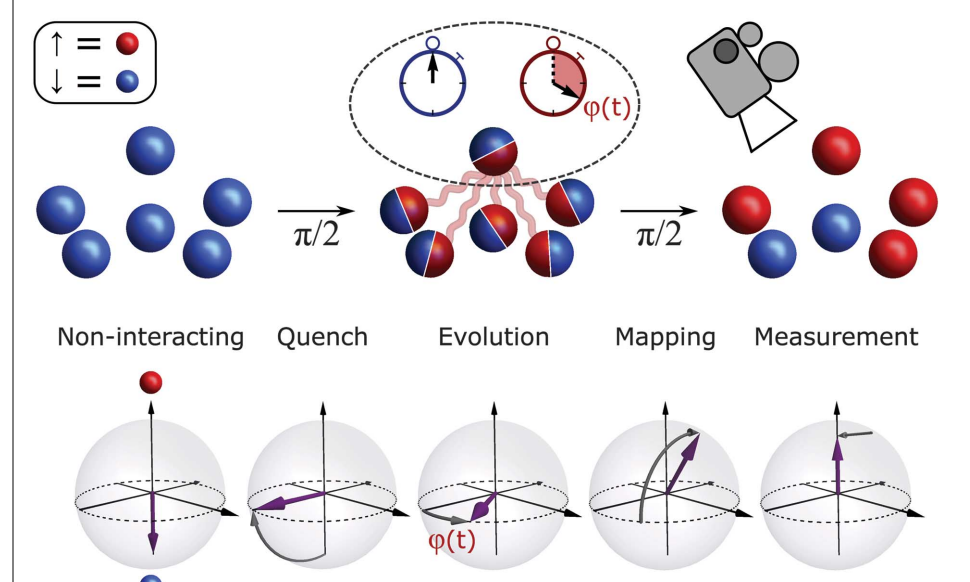


**Fig. 1. Ramsey interferometry of a many-body system.** The first  $\pi/2$  pulse puts each atom in a superposition of ↑ (red) and  $\downarrow$  (blue) states. Strong interactions between the red components cause the relative phase of the superposition to advance by  $\varphi$ , as indicated by the blue and red clocks. The second  $\pi/2$  pulse maps  $\varphi$  onto spin polarization, which is measured by absorption imaging. The duration of each  $\pi/2$  pulse is 17  $\mu$ s, and the evolution time between the pulses is varied between 40 and 130  $\mu$ s. Below, the stages of our protocol are illustrated in terms of the collective spin on the Bloch sphere; the purple arrow denotes the collective Bloch vector, and its motion is indicated by the gray arrows.

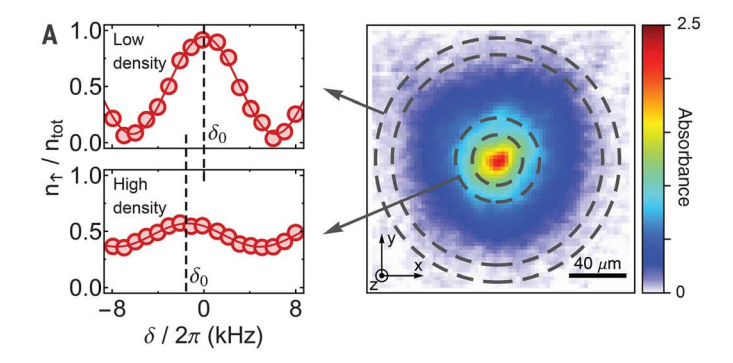


Fig. 2. Density-dependent phase winding. (A) Ramsey oscillations of the spin-↑ density as a function of the RF detuning δ. Oscillations at different positions in the trap reveal the density dependence of  $\varphi$ . Strong interactions both shift the center of the Ramsey fringes,  $\delta_0$ , and reduce their contrast. (**B**) For weak interactions (top and bottom),  $\Omega$  varies linearly with density, but close to unitarity (middle), it shows nonlinear behavior that reveals the influence of three-body physics. At all scattering lengths, the data are fitted well by a second-order polynomial (solid blue lines); the red dashed lines show the linear parts of the fits.  $\Omega$ was obtained from the measured  $\delta_0$  by setting  $\Omega = -\delta_0$ , and the error bars show standard errors in the fitted center of the corresponding Ramsey fringes.

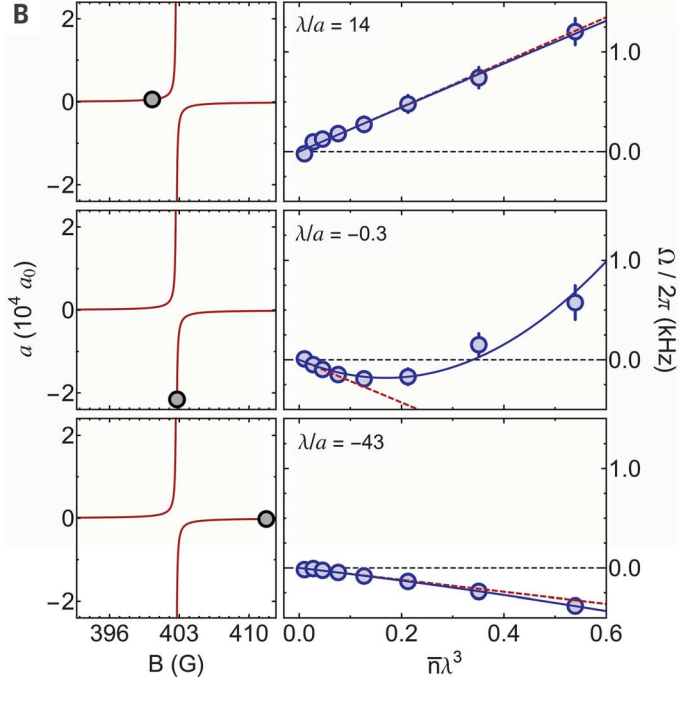
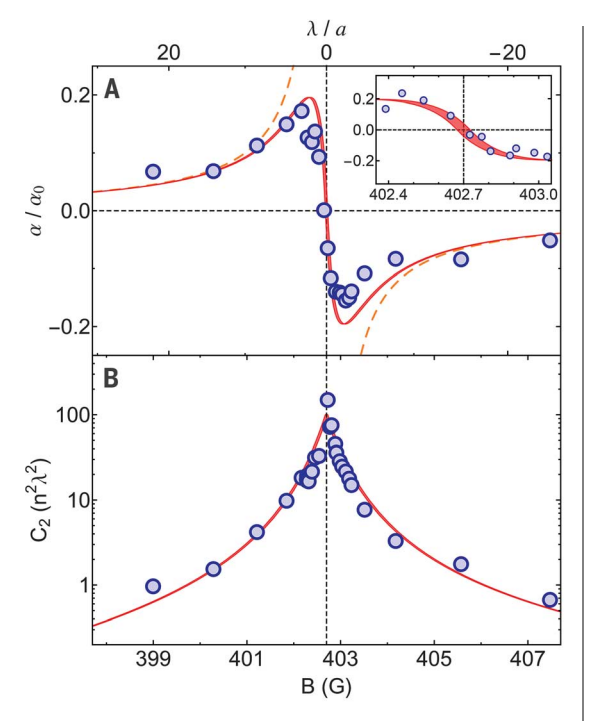


Fig. 3. Two-body contact. (A) Initial slope  $\alpha$  of  $\Omega(\overline{n})$ , normalized to  $\alpha_0$  =  $8\pi\hbar\lambda/m$ . The solid red line shows the theoretical prediction (34), and the dashed orange line shows its weakly interacting limit,  $\alpha/\alpha_0 = \alpha/\lambda$ . The dashed black vertical line shows the Feshbach resonance position. Inset, measurements close to the resonance. (**B**)  $C_2$  extracted from  $\alpha$ . The red line is the theoretical prediction of (35). The thickness of the red lines reflects the uncertainty in  $B_0$ . In both plots, the error bars are smaller than the point size.



where m is the atom mass, n the density of the  $\uparrow$ component, and a the  $\uparrow \uparrow$  scattering length. Away from unitarity,  $C_2 \propto n^2 a^2$  and  $C_3 \propto n^3 a^4$  (19, 20), and the ratio of the  $C_3$  and  $C_2$  contributions to  $\Omega$  is of the order of  $n|a|^3 \ll 1$ . At unitarity, both contacts saturate at their maximal values; in a thermal gas,  $C_2 \propto n^2 \lambda^2$  and  $C_3 \propto n^3 \lambda^4$ , where  $\lambda$  is the thermal wavelength. The crucial advantage of using the precession of the Bloch vector to observe three-particle correlations is that the  $C_2$  contribution to  $\Omega$  vanishes at unitarity (where  $|a| \to \infty$ ).

Our experimental setup is described in (32). We worked with 39K atoms prepared in an optical harmonic trap with frequencies ( $\omega_x$ ,  $\omega_y$ ,  $\omega_z$ )/ $2\pi$  = (48.5, 56.5, 785) Hz. Our two spin states, labeled in the low-field basis, were  $|\uparrow\rangle=|F=1,m_F=1\rangle$ and  $|\downarrow\rangle = |F = 1, m_F = 0\rangle$ . We tuned the  $\uparrow\uparrow$  scattering length a by using a Feshbach resonance centered on a magnetic field of  $B_0$  = 402.70(3) G (30). In all our experiments,  $|a| > 300a_0$ , whereas the moduli of the ↑↓ and ↓↓ scattering lengths are <10 $a_0$  (33), where  $a_0$  is the Bohr radius. Near  $B_0$ , the bare splitting of the  $\uparrow$  and  $\downarrow$  states is

≈99 MHz. We prepared clouds at the critical point for Bose-Einstein condensation, with a phase-space density  $n_{\rm tot}\lambda^3\approx 2.6$  at the trap center, where  $n_{\rm tot}$  is the number density, and the cloud temperature of 370 nK corresponds to  $\lambda \approx$  $8600a_0$ . The duration of each  $\pi/2$  pulse was  $t_p =$ 17 µs, and the evolution time between the pulses, T, was varied between 40 and 130  $\mu$ s. At the end of the whole Ramsey sequence, we measured the fractional  $\uparrow$  population,  $n_{\uparrow}/n_{\text{tot}}$ , by in situ absorption imaging along the axial direction,  $\hat{z}$ (Fig. 2A). In Bose gases, strong coherent interactions are generally accompanied by substantial inelastic losses, but on the time scale of our experiments, the atom loss at our highest density was <10%.

To measure the density-dependent  $\Omega$ , we scanned the detuning of the RF source from the noninteracting resonance, observed Ramsey oscillations of the spin populations, and extracted the detuning for which  $n_1/n_{\rm tot}$  is maximal,  $\delta_0$  (Fig. 2A). We exploited the fact that the atoms are essentially stationary during the Ramsey sequence to simultaneously extract  $\delta_0$  for a wide range of densities from the local oscillations of  $n_{\uparrow}/n_{\rm tot}$  in different regions of the cloud. Generally

$$\delta_0 = -\frac{\varphi + \Delta \varphi_p}{T + 4t_p/\pi} \tag{2}$$

where  $\Delta\phi_p$  is any interaction-induced phase accumulated during the RF pulses (30). For constant  $\Omega$  (so  $\varphi = \Omega T$ ) and  $T \gg t_{\rm p}$ , Eq. 2 reduces to the intuitive  $\delta_0 = -\Omega$ . For measurements at low density and away from unitarity, this is an excellent approximation. For more accurate studies at high densities or close to unitarity, we performed differential measurements, in which we extracted  $\delta_0$  for various evolution times

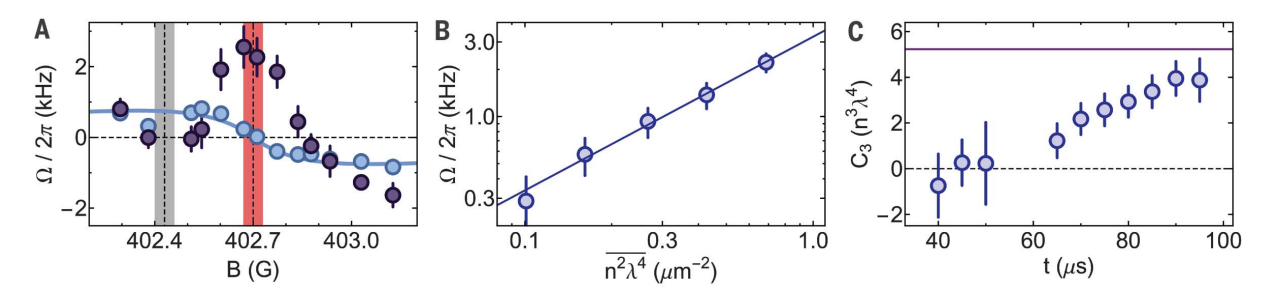


Fig. 4. Three-body contact. (A)  $\Omega$  at t=90 μs, for densities  $\overline{n}\lambda^3=0.13$  (light blue) and  $\overline{n}\lambda^3=0.54$  (purple). For reference, we also show the two-body prediction for the lower-density data (blue line). The red band indicates the position of the Feshbach resonance, and the gray band shows the location of the previously observed minimum in the three-body loss rate (23). (B) Log-log plot of the density dependence of  $\Omega(B_0)$ ;  $t = 90 \,\mu s$  data are averaged within the red band shown in (A). The linear fit (blue line) gives a slope  $\gamma = 1.0(1)$ , in excellent agreement with the three-body scaling law. (C) The threebody contact density  $C_3$  as a function of time after the interaction quench. The horizontal purple line shows the theoretical prediction for the equilibrium unitary Bose gas (20).

and reconstructed the instantaneous  $\Omega(t)$ . This mitigated the small effects of the nonzero pulse duration and also allowed us to study the dynamics of  $C_2$  and  $C_3$ . The longest time over which we can study the contact dynamics is limited by the decay of the Ramsey fringe contrast at high density, caused by interatomic collisions and the inhomogeneous dephasing along the imaging line of sight.

In Fig. 2B, we show the density dependence of  $\Omega$  (assuming for now  $\Omega = -\delta_0$ ) for weak and nearly unitary interactions.  $\overline{n}$  is the  $\uparrow$  density experienced by an atom, averaged over the imaging line of sight and a small radial bin in the image plane (30). For weak interactions,  $\Omega \propto \overline{n}$ , consistent with the expected dominance of two-body correlations for  $n|a|^3 \ll 1$ . However, close to unitarity,  $\Omega(\overline{n})$  is nonlinear and even changes sign, which cannot be explained by two-body physics.

For a quantitative analysis, we first focused on very low densities. In this limit,  $\Omega$  is dominated by two-body correlations at all interaction strengths. From the measurements of  $\Omega(\overline{n})$ , we extracted the initial slope  $\alpha=\partial\Omega/\partial\overline{n}|_{\overline{n}=0}$  (Fig. 2B), which gives the behavior of  $\Omega$  at vanishing density.

In Fig. 3A, we plot  $\alpha$  across the Feshbach resonance for  $T = 125 \,\mu s$ . The solid red line shows  $\alpha = 8\pi\hbar \overline{\Re(f)}/m$ , where  $\overline{\Re(f)}$  is the real part of the scattering amplitude f(34), averaged over the thermal momentum distribution, and  $\hbar$  is the reduced Planck constant; the dashed orange line is the weakly interacting limit  $\alpha =$  $8\pi\hbar a/m$ . Using Eq. 1, from our measurements, we extracted  $C_2/n^2 = \alpha 4\pi ma/\hbar$ . This is plotted in Fig. 3B, along with an analytic prediction for  $C_2$  (35). Over two orders of magnitude in  $C_2$ , we find excellent agreement between theory and our data.

In our search for  $C_3$ , a key prediction of Eq. 1 is that the  $C_2$  contribution to  $\Omega$  vanishes exactly at  $B_0$ . In the inset of Fig. 3A, we show measurements focused on the resonance region and verify that this is indeed the case. Here, we measured  $\delta_0$  for two evolution times,  $T_1$  = 40  $\mu s$ and  $T_2$  = 125 µs, to assess the instantaneous  $\Omega$  at  $t = 82.5 \,\mu s$  according to Eq. 2. We also varied  $T_1$  and  $T_2$  and found that  $\alpha$  is always consistent with the equilibrium theory curve (red shading). This is in agreement with our simulations of the two-particle dynamics after an interaction quench (30). We theoretically find that  $C_2$ equilibrates on a time scale  $\tau_2$ , which is  $\approx ma^2/\hbar$ away from the Feshbach resonance and  $\approx m\lambda^2/\hbar$ at unitarity; for our experimental parameters,  $\tau_2$ is shorter than the first RF pulse.

We next turned to higher densities and strong interactions, where the effect of  $C_3$  should be prominent. We always reconstructed the instantaneous  $\Omega(t)$ , and in Fig. 4A, we show it for t =90 us and two different densities. At high density, a nonzero  $\Omega$  at unitarity is evident, which, per Eq. 1, cannot arise from a  $C_2$  contribution [see also (36, 37)]. Additionally, away from unitarity, at  $B < B_0$ , an intriguing suppression of  $\Omega$  is apparent, which coincides with the previously observed strong suppression of three-body losses (at  $a \approx 5600a_0$ ) (23), qualitatively associated with atom-dimer physics (38).

We focused on the nonzero  $\Omega$  at unitarity and verified that it arises from three-particle correlations by looking at its scaling with density. According to Eq. 1, a  $C_3$  contribution to  $\Omega$  should scale linearly with  $n^2\lambda^4$ . In Fig. 4B, we show that  $\log[\Omega(B_0)]$  is linearly dependent on  $\log(n^2\lambda^4)$ , confirming a power-law scaling (30). To determine the exponent itself, we fitted a line to the data and extracted the slope  $\gamma = d(\log\Omega)/d[\log(n^2\lambda^4)]$ . We find  $\gamma = 1.0(1)$ , which is in excellent agreement with the predicted three-body scaling.

Last, we studied the value of the unitary  $C_3$ . In contrast to  $C_2$ , we observed a gradual development of  $C_3$  over the time scale of our experiment (Fig. 4C), which means that after the interaction quench, the three-body correlations develop slower than the two-body ones. For  $t \lesssim 50 \,\mu\text{s}$ , the three-body contact is consistent with zero (within our error bars), whereas at our longest times,  $t \approx$ 100 µs, it approaches the theoretical expectation for the equilibrium unitary gas,  $C_3/(n^3\lambda^4) \approx$ 

Our measurements provide a conclusive observation of the effects of three-body correlations on the coherent behavior of an atomic Bose gas. The nonequilibrium dynamics of the three-body contact are an interesting open problem for future study. It would be exciting to extend our technique to a deeply degenerate gas, for which  $C_3$  is not even theoretically known (20). In our harmonic trap setup, starting with a noninteracting Bose condensate would result in prohibitively short lifetimes after the quench to unitarity, but this problem could be mitigated by using a uniform trapping potential (39).

#### **REFERENCES AND NOTES**

- 1. C. Chin, R. Grimm, P. Julienne, E. Tiesinga, Rev. Mod. Phys. 82, 1225-1286 (2010)
- M. Inguscio, W. Ketterle, C. Salomon, Eds., Ultracold Fermi Gases (Proceedings of the International School of Physics "Enrico Fermi," Course CLXIV, Varenna, Italy, 20 to 30 June 2006 IOS Press 2007)
- W. Zwerger, Ed., BCS-BEC Crossover and the Unitary Fermi Gas, vol. 836 of Lecture Notes in Physics (Springer, 2011).
- M. W. Zwierlein, in Novel Superfluids, vol. 2, K.-H. Bennemann, J. B. Ketterson, Eds. (Oxford Univ. Press, 2014), chap. 18.
- B. S. Rem et al., Phys. Rev. Lett. 110, 163202 (2013).
- R. J. Fletcher, A. L. Gaunt, N. Navon, R. P. Smith, Z. Hadzibabic, Phys. Rev. Lett. 111, 125303 (2013).
- P. Makotyn, C. E. Klauss, D. L. Goldberger, E. A. Cornell, D. S. Jin, Nat. Phys. 10, 116-119 (2014).
- U. Eismann et al., Phys. Rev. X 6, 021025 (2016).
- M.-G. Hu et al., Phys. Rev. Lett. 117, 055301 (2016).
- 10. N. B. Jørgensen et al., Phys. Rev. Lett. 117, 055302
- 11. F. Chevy, C. Salomon, J. Phys. At. Mol. Opt. Phys. 49, 192001 (2016).
- 12. S. Tan, Ann. Phys. 323, 2952-2970 (2008).
- 13. M. Punk, W. Zwerger, Phys. Rev. Lett. 99, 170404 (2007).
- 14. G. Baym, C. J. Pethick, Z. Yu, M. W. Zwierlein, Phys. Rev. Lett. 99, 190407 (2007).
- 15. E. Braaten, D. Kang, L. Platter, Phys. Rev. Lett. 104, 223004
- 16. W. Schneider, M. Randeria, Phys. Rev. A 81, 021601 (2010).
- 17. Y. Castin, C. Mora, L. Pricoupenko, Phys. Rev. Lett. 105, 223201 (2010).
- 18. E. Braaten, D. Kang, L. Platter, Phys. Rev. Lett. 106, 153005 (2011).
- 19. F. Werner, Y. Castin, Phys. Rev. A 86, 053633 (2012).
- 20. D. H. Smith, E. Braaten, D. Kang, L. Platter, Phys. Rev. Lett. 112, 110402 (2014).
- 21. V. Efimov, Phys. Lett. B 33, 563-564 (1970).
- 22. T. Kraemer et al., Nature 440, 315-318 (2006).
- 23. M. Zaccanti et al., Nat. Phys. 5, 586-591 (2009).
- 24. F. Ferlaino et al., Few-Body Syst. 51, 113-133 (2011).
- 25. R. J. Wild, P. Makotyn, J. M. Pino, E. A. Cornell, D. S. Jin, Phys. Rev. Lett. 108, 145305 (2012).

- 26. O. Machtey, Z. Shotan, N. Gross, L. Khaykovich, Phys. Rev. Lett. 108, 210406 (2012).
- 27. S. Roy et al., Phys. Rev. Lett. 111, 053202 (2013).
- 28. S. Piatecki, W. Krauth, Nat. Commun. 5, 3503 (2014).
- 29. M. Barth, J. Hofmann, Phys. Rev. A 92, 062716 (2015).
- 30. Materials and methods are available as supplementary materials.
- 31. M. Cetina et al., Science 354, 96-99 (2016).
- 32. R. L. D. Campbell et al., Phys. Rev. A 82, 063611 (2010).
- M. Lysebo, L. Veseth, *Phys. Rev. A* **81**, 032702 (2010).
   S. J. J. M. F. Kokkelmans, B. J. Verhaar, K. Gibble, D. J. Heinzen, Phys. Rev. A 56, R4389-R4392 (1997).
- 35. E. Braaten, H.-W. Hammer, J. Phys. B 46, 215203 (2013).
- 36. W. Li, T.-L. Ho, Phys. Rev. Lett. 108, 195301 (2012).
- 37. H. T. C. Stoof, J. J. R. M. van Heugten, J. Low Temp. Phys. 174, 159-183 (2014).
- 38. The effect of atom-dimer physics on spectroscopy has also been observed in Fermi systems (40).

- 39. A. L. Gaunt, T. F. Schmidutz, I. Gotlibovych, R. P. Smith, Z. Hadzibabic, Phys. Rev. Lett. 110, 200406 (2013).
- 40. M. Jag et al., Phys. Rev. Lett. 112, 075302 (2014).

#### **ACKNOWLEDGMENTS**

We are indebted to E. Braaten for his crucial input toward the derivation of the numerical prefactors in Eq. 1 and a critical reading of the manuscript. We thank M. Robert de Saint Vincent for contributions in the early stages of the project, M. Sohmen for experimental assistance, and S. Kokkelmans, E. Cornell, D. Papoular, F. Werner, I. Bouchoule, I. Chuang, and J. Dalibard for helpful discussions. This work was supported by the U.K. Engineering and Physical Sciences Research Council (grant no. EP/N011759/1), the European Research Council (OBox), the U.S. Army Research Office (ARO), and the U.S. Air Force Office of Scientific Research (AFOSR), N.N. acknowledges support from Trinity College, Cambridge; R.P.S.

from the Royal Society; R.L. from the European Union Marie Curie program (grant no. MSCA-IF-2015 704832); and M.W.Z. from the AFOSR Multidisciplinary University Research Initiative on exotic quantum phases, U.S. NSF, and ARO. Data supporting this publication are available for download at https://doi.org/10.17863/CAM.7184.

#### SUPPLEMENTARY MATERIALS

www.sciencemag.org/content/355/6323/377/suppl/DC1 Materials and Methods Supplementary Text Figs. S1 to S4 Table S1 References (41-47)

16 August 2016: accepted 22 December 2016 10 1126/science aai8195



### Two- and three-body contacts in the unitary Bose gas

Richard J. Fletcher, Raphael Lopes, Jay Man, Nir Navon, Robert P. Smith, Martin W. Zwierlein and Zoran Hadzibabic

Science **355** (6323), 377-380. DOI: 10.1126/science.aai8195

Elusive three-body matters

Tunable interactions make dilute atomic gases ideal for studying the collective dynamics of many-body systems. If the gas consists of strongly interacting fermions evenly divided into two groups of opposite spin, many of its properties can be distilled to two-body correlations. Fletcher *et al.* show that this does not hold for a gas of bosons, where identical particles happily congregate. The researchers measured a quantity that, in a thermal resonantly interacting Bose gas, depends only on three-body correlations. This enabled them to quantify the elusive correlations and establish unambiguously their effect on the physics of the many-body state.

Science, this issue p. 377

ARTICLE TOOLS http://science.sciencemag.org/content/355/6323/377

SUPPLEMENTARY http://science.sciencemag.org/content/suppl/2017/01/25/355.6323.377.DC1 MATERIALS

REFERENCES This article cites 41 articles, 1 of which you can access for free

http://science.sciencemag.org/content/355/6323/377#BIBL

PERMISSIONS http://www.sciencemag.org/help/reprints-and-permissions

Use of this article is subject to the Terms of Service